



Effect of COVID-19 epidemic-led lockdowns on aerosol black carbon concentration, sources and its radiation effect in northeast India

SAMEER SINGH and SHARAD GOKHALE*

Department of Civil Engineering, Indian Institute of Technology Guwahati, Guwahati 781 039, India.

*Corresponding author. e-mail: sharadbg@iitg.ac.in

MS received 31 May 2021; revised 25 January 2022; accepted 27 January 2022

The COVID-19 epidemic-led lockdown (LD) from March 25 to May 31, 2020, had a different level of impact on air quality in the ecologically sensitive region of northeast India, even though the restriction on main anthropogenic activities was expected to reduce particulate matter concentration. The daily average black carbon concentration measured at 880 nm (BC_{880}) was $1.5\text{--}15.6 \mu\text{g m}^{-3}$ (mean: $5.75 \pm 4.24 \mu\text{g m}^{-3}$) during the measurement period. It was $9.29 \pm 4.11 \mu\text{g m}^{-3}$ during pre-LD (February 12–March 21), $4.70 \pm 0.95 \mu\text{g m}^{-3}$ during LD1 (March 25–April 14), $3.41 \pm 0.56 \mu\text{g m}^{-3}$ during LD2 (April 15–May 3), $3.69 \pm 1.50 \mu\text{g m}^{-3}$ during LD3 (May 4–17), $2.94 \pm 0.93 \mu\text{g m}^{-3}$ during LD4 (May 18–31), and $6.56 \pm 5.35 \mu\text{g m}^{-3}$ during the Post-LD (June 6–July 3) of 2020. It decreased up to 68% during the lockdowns. The source apportionment based on an improved method showed a significant improvement in the contribution of BC_{880} sources. The radiation effect determined by Angstrom Absorption Exponent showed that brown carbon accounted for 25% of the aerosol light absorption at 370 nm during the lockdown period. Relative humidity correlates substantially with BC_{880} , while rainfall, temperature, and solar radiation were negatively correlated. The bivariate analysis showed the dominance of local emissions in the BC_{880} concentrations.

Keywords. Aethalometer; black carbon; COVID-19 epidemic; lockdown; radiation effect; source apportionment.

1. Introduction

The World Health Organization (WHO) acknowledged the COVID-19 pandemic as a worldwide health disaster affecting society, the economy, and the environment. The COVID-19 virus can remain viable for up to 3 days on plastic and stainless steel and 3 hours on aerosols (Stanam *et al.* 2020). Black Carbon (BC) is the finer constituent of

atmospheric aerosol. It acts as the carrier of viruses and wide-ranging chemicals of varying toxicity to the human body besides its role in the climate forcing (WHO *et al.* 2012; Wang *et al.* 2014). It is linked to the atmospheric environment through different physicochemical and biological processes. It travels a long distance in ambient air quickly due to its smaller size (Ramanathan and Carmichael 2008). Epidemiological studies have shown the

association of cardiopulmonary mortality and morbidity with exposure to BC, causing a public health problem, including premature deaths of vulnerable groups (Jansen *et al.* 2005). Some studies have reported the typical health effects of BC in equivalent amounts of daily passively-smoked cigarettes (Van der Zee *et al.* 2016; Singh and Gokhale 2021). Hence, reducing human exposure to BC would mitigate its impacts on their health.

Climate change affects global diversity (Beyer *et al.* 2021). Bats are the probable zoonotic cause of both SARS-CoV-1 and SAR-CoV-2 (recognized as COVID-19 pandemic), which result in severe critical respiratory syndrome from wildlife (agricultural animals) to humans (Banerjee *et al.* 2019; Beyer *et al.* 2021; Xiao *et al.* 2020), indicating a link between BC and Coronavirus. The number of CoVs numbers existing in a region is strongly linked with native bat species, and is influenced by climatic situations that drive species' geographical dispersals (Beyer *et al.* 2021). The early studies on the COVID-19 epidemic impacting airborne and water quality are reported in the recent literature (Ahmed *et al.* 2020; Chauhan and Singh 2020; Chowdhuri *et al.* 2020; Kumari and Toshniwal 2020; Mahato *et al.* 2020; Ranjan *et al.* 2020; Goel *et al.* 2021; Gogoi *et al.* 2021; Pathak *et al.* 2021; Saxena and Raj 2021; Sharma *et al.* 2020; Westhaus *et al.* 2021; Zhang *et al.* 2021), while BC and BrC with radiation effects are not studied yet. BC is the next most climate driving agent present in the atmosphere after CO₂ (Ramanathan and Carmichael 2008). Climate change might cause the evolution and spread of the two SARS coronaviruses (CoVs) (Banerjee *et al.* 2019).

BC has significant negative influences on climate and human health (Singh and Dey 2012; Bond and Bergstrom 2006). It has a considerable warming potential with the rate of warming changes with location and elevation (Ramanathan and Carmichael 2008). The mountainous and hilly topography experience additional quick variations in temperature than surroundings at minor peaks (Goldreich *et al.* 1986). Almost 70% of the region in northeast India is under a hilly ecosystem where alpine vegetation, snow-capped high mountains (1–5 km a.s.l.), and rocky surface dominate the physical landscape (Gogoi *et al.* 2009; Pathak *et al.* 2021). Thus, hilly regions with considerable human settlements may substantially impact the BC and its contribution to light absorption. BC is a primary product of incomplete burning of biomass

and fossil fuel. Traffic contributes to about 33–90% BC emission in areas with rich vehicular activities and congestion (Schneider *et al.* 2008; USEPA 2012). About 8% comes from the open burning of biomass (Reid *et al.* 2004). The traffic-originated BC particles are blacker than the particles from biomass combustion, hence having higher warming effects (Han *et al.* 2007; Ramanathan and Carmichael 2008). Diesel engines produce a relatively high amount of BC (Evans *et al.* 2017). It is a primary pollutant, so its concentration in the atmosphere is directly linked to anthropogenic activities.

The current COVID-19 pandemic forced partial or complete lockdown leading to the sudden closure of anthropogenic activities. The lockdowns were lifted gradually, and the actions were successively increased. The COVID-19 epidemic has triggered nearly 3 million deaths worldwide, and over 145 million confirmed cases (<https://covid19.who.int/>). To contain the spread of COVID-19 in India, a countrywide lockdown was forced in different periods starting March 25 to May 31, 2020. During the lockdown, the total or partial shutdown of anthropogenic activities (stone quarries, road construction, open burning of biomass, hill cutting, vehicular movement, etc.) improved the air quality concerning PM_{2.5}, PM₁₀ (particulate matter <2.5 and <10 μm), BC, NO₂, SO₂, CO, NH₃, and O₃ pollutants in Indian megacities, e.g., New Delhi (National capital region), Kolkata (Eastern India), Mumbai (Southern India) (Chowdhuri *et al.* 2020; Kumari and Toshniwal 2020; Mahato *et al.* 2020; Goel *et al.* 2021) and PM_{2.5} worldwide (Chauhan and Singh 2020). The lockdown also reduced India's aerosol optical depth (AOD); nearly 45% of the AOD dropped during lockdown periods (Ranjan *et al.* 2020). In a study by Mahato *et al.* (2020), PM₁₀ and PM_{2.5} concentrations decreased by about 60% and 40%, respectively, throughout the initial lockdown (LD1: March 25–April 14) in the National capital region (Delhi) as compared to 2019. Chowdhuri *et al.* (2020) reported a significant decrease in lightning flash by about 49% in summer because of the lockdown in Kolkata, India. Pathak *et al.* (2021) assessed the impacts of lockdown over the upper Brahmaputra river basin (Dibrugarh) of northeast India and observed that the air quality in respect of O₃, NO₂, NO_x, CO, SO₂, PM₁₀, PM_{2.5}, PM₁, and BC improved moderately during lockdowns as compared to the same period of 2015–2019. Gogoi

et al. (2021) reported a decrease in BC by about 60% and about 30% over Indo-Gangetic plains (IGPs) and northeastern India, respectively, during LD2. It also found that the BC was high over the IGPs and northeast India compared to the rest of India. The COVID-19 amid lockdown also reduced the air impurity levels (by 30–50%) in the neighbouring region (southwestern China) (Chen *et al.* 2020) and other areas in the world (Chauhan and Singh 2020).

Guwahati is the largest and fastest-growing city in northeast India. It is situated in a small to the steep-sloped hilly region of the lower Brahmaputra river basin, where fossil fuel (road traffic and small industries) and biomass burning (wood burning and forest fires) are the leading sources of BC (Chakrabarty *et al.* 2012; Barman and Gokhale 2019; Singh and Gokhale 2021). Barman and Gokhale (2019) showed that in Guwahati, traffic and biomass contribute 85–92% and 9–15%, respectively, to the total BC. While in a study of source apportionment to increase the accuracy of contributions by using site-specific properties, the contributions were found to be 70% and 30% from traffic and biomass during the winter season in this region (Singh and Gokhale 2021). This study has been carried out to determine the impacts of lockdown in different phases on BC_{880} and BrC originated in this hilly region of northeast India and its effects on light absorptions. Given the significant biomass burning in the area in the winter season, the results have been analyzed to see how total or partial reduction of fossil fuel consumption has influenced the trend of BC_{880} . A seven discrete wavelength Aethalometer utilizing dual spot technology was used for BC measurements, and source apportionment was done as per the AE33 method (Sandradewi *et al.* 2008). The research results in this region's unique geography and environment would contribute to the recent literature on COVID-19 associated air pollution studies.

2. Methodology

The real-time BC concentrations were measured in a rural-industrial region of North Guwahati at Air and Noise Pollution Laboratory of the Indian Institute of Technology Guwahati (IITG, 26.1878°N, 91.6916°E, elevation: 56 m asl) from 12th February to 3rd July 2020 (figure 1). A seven-

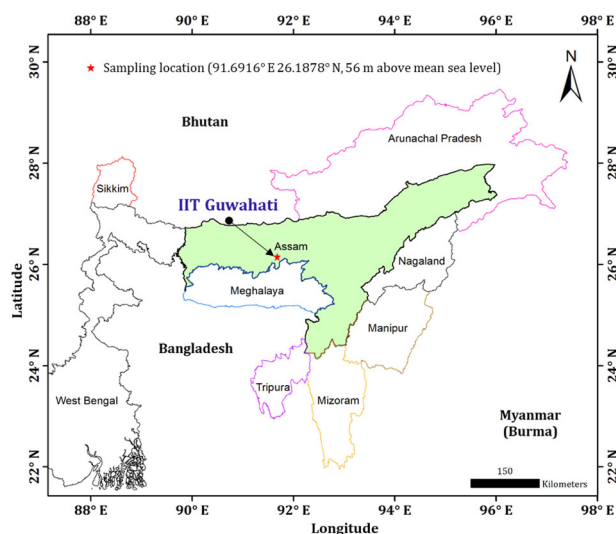


Figure 1. The location of IIT Guwahati (XY, solid red star) in Assam, northeast India.

channel Aethalometer (Model Number: AE-33, Magee Scientific Inc.) was set up on the top floor (nearly 12 m high), operated at two liters per minute with a waterproof $PM_{2.5}$ inlet attached on the top of the inlet tube at a one-min interval. A TFE coated glass fiber filter tape roll (30 mm × 30 ft., Part No. 8050) was used. There are cement and brick kilns industries in the surrounding area along the trafficked national highways, NH27 at about 2 km to the west and NH427 at about 250 m to the south. A wireless weather station was (model: Davis Vantage Pro2, California, USA) installed in the same building to collect the meteorological parameters. It was located on the top floor to confirm that no hindrance weakens the measurements. Data were recorded at the 5-min interval, including atmospheric temperature (AT: °C), precipitation or rainfall (RF: mm), surface-reaching solar radiation (SR: $W m^{-2}$), relative humidity (RH: %), wind speed (WS: $m s^{-1}$), wind direction (WD: °), and barometric pressure (BP: mbar). Davis Vantage Pro2 weather station is capable of measuring the pre-tested values of meteorological parameters with maximum accuracy as: AT (0.1°C precision ± 0.5°C), RH (1%RH precision ± 3%RH), RF (214 cm^2 collector with 0.2 mm bucket), WS (0.4 ms^{-1} steps ± 5%), WD (16-point compass), BP (internal console ± 1.0 mbar), and SR (detects SR at wavelengths of 300–1100 nm ± 5%) which is also capable of transferring the recorded data to the console unit placed up to 300 m distance (Jenkins 2014). The sunshine hour is essential in estimating the surface-reaching solar radiation. In this study, seven sunshine hours per

day (09:00–16:00) were considered. To avoid interruption in the power supply, a car battery (12 V, three nos.) was attached to an AC to DC signal inverter, which powered the instruments for 15 min during the electricity interruption period.

The COVID-19 lockdown stopped all anthropogenic activities that improved India's air quality (Mahato *et al.* 2020; Pathak *et al.* 2021; Zhang *et al.* 2021). Northeast India has several anthropogenic sources, including one coal-fired power plant (Bongaigaon Thermal Power Station), 110 large scale and 102 medium-scale (<https://industries.assam.gov.in/portlets/industry-in-assam>) industries (refinery, bottling plant, fertilizer, metal alloy, cement, paper, and board mill, etc.) in diverse topographical areas of this region, significantly influence the ambient air quality. The number of on-road automobiles in Assam has increased from 0.53 million in 2001 to 2.84 million in 2018 (Economic survey of Assam 2017–2018). Previous studies reported on-road traffic as a dominant source of BC in the Brahmaputra River valley region (Barman and Gokhale 2019; Singh and Gokhale 2021). The vehicles plying on the roads of Guwahati are all mixed in the various proportion of BS-II, BS-III, and BS-IV compliant. Besides, a 972-km Indian railway network across the northeastern states is diesel power-driven, which significantly contributes to the atmospheric BC.

To control the COVID-19 epidemic, a lockdown in northeast India was announced by the Indian Government. The lockdown in four phases and the limitations in several activities started from 24th March to 31st May 2020. Each stage had a different relaxation scale in several essential activities such as public transportation and essential industries' opening. Hence, the sampling was also done in six different stages: pre-lockdown (February 12–March 21), lockdown 1 (March 25–April 14), lockdown 2 (April 15–May 3), lockdown 3 (May 4–17), lockdown 4 (May 18–31), and post-lockdown (June 7–July 3 2020). The lockdown period was divided into different phases based on the measures taken and the standard operating procedures issued by the Indian Government to extend the lockdowns from time to time, depending upon the situation of the pandemic. During this period (February–July), the mean daily minimum and maximum temperatures varied from 14.80 to 21.65°C (mean: 19.39 ± 2.78°C) and 26.69 to 35.06°C (mean: 28.19 ± 2.98°C), correspondingly, with total precipitation of 101 mm. The mean RH

was more in LD4 (86 ± 2%) and lower in LD1 (78 ± 7%), while the total of sunny daylight hours was almost similar. The mean WSs in LD2 (2.38 ± 0.61 m s⁻¹) were more than twice the pre-LD (0.99 ± 0.36 m s⁻¹) period.

The Aethalometer (AE33) model measures light reduction at seven discrete wavelengths (950, 880, 660, 590, 520, 470, 370 nm) using the in-built dual spot technology (Drinovec *et al.* 2015; Goel *et al.* 2021) and the hourly-average BC concentrations were estimated at 880 nm (BC₈₈₀). The absorption angstrom exponent (AAE) was calculated from the coefficient of aerosol absorption (denoted as b_{abs}). It is a product of aerosol BC mass concentration and mass absorption cross-section (MAC) (Dumka *et al.* 2018). The MAC values of 18.47, 14.54, 7.77, and 7.19 m² g⁻¹, correspondingly, were used for 370, 470, 880, 950 nm wavelengths (Drinovec *et al.* 2015). The AAE₃₇₀₋₈₈₀ values were estimated from the resulting $b_{\text{abs}}(\lambda)$ for the wavelength pair of 370 and 880 nm by equations (1 and 2) (Sandradewi *et al.* 2008).

$$b_{\text{abs}(\lambda)} = BC_{\lambda} \times MAC_{\lambda}, \quad (1)$$

$$AAE = -\frac{\ln(b_{\text{abs}(1)}/b_{\text{abs}(2)})}{\ln(\lambda_1/\lambda_2)}, \quad (2)$$

where $b_{\text{abs}(1)}$ and $b_{\text{abs}(2)}$ are the coefficients of aerosol absorption (b_{abs}) at two distinct wavelengths.

The two-component mixing (AE33) model was used for the source apportionment of BC from two primary sources associated with biomass and fossil fuel burning, taking AAE of fossil fuel as 1.0 and biomass as 1.7 (Singh and Gokhale 2021). If AAE_{FF} as 1.0 and AAE_{BB} as 2.0 are applied according to the previous studies (Barman and Gokhale 2019; Tiwari *et al.* 2015), then biomass and FF burning involved are calculated consistently with the six distinct phases of lockdowns, as presented in figure S1. Several studies have reported the spectral band 370–880 nm wavelength for the segregation of BC sources (Dumka *et al.* 2018; Chen *et al.* 2020; Goel *et al.* 2021). The source apportionment of BC was done with the support of equations (3–9), with the b_{abs} estimated at 370 and 880 nm. The b_{abs} were evaluated by the BC mass concentrations at 370 and 880 nm using equation (1). The Aethalometer model (AE33) assumes that BC originated simply from biomass and fossil fuel burning sources, as equation (3).

$$BC = BC_{FF} + BC_{BB}. \quad (3)$$

The b_{abs} for the wavelength of 370 and 880 nm are separated as indicated by equations (4 and 5) (Sandradewi *et al.* 2008).

$$b_{abs_370} = b_{abs_FF_370} + b_{abs_BB_370}, \quad (4)$$

$$b_{abs_880} = b_{abs_FF_880} + b_{abs_BB_880}. \quad (5)$$

Equations (4–7) were used to calculate FF and BB’s light absorption at 370 and 880 nm wavelength. The AAE_{FF} and AAE_{BB} values as 1.0 and 1.7 were initially used in equations (6 and 7).

$$\frac{b_{abs_FF_370}}{b_{abs_FF_880}} = \left(\frac{370}{880}\right)^{-AAE_{FF}}, \quad (6)$$

$$\frac{b_{abs_BB_370}}{b_{abs_BB_880}} = \left(\frac{370}{880}\right)^{-AAE_{BB}}. \quad (7)$$

The BC_{FF} and BC_{BB} mass concentrations (at 880 nm) were estimated by equations (8 and 9).

$$BC_{FF_880} = \frac{b_{abs_FF_880}}{MAC_{(880\text{ nm})}}, \quad (8)$$

$$BC_{BB_880} = \frac{b_{abs_BB_880}}{MAC_{(880\text{ nm})}}. \quad (9)$$

Considering that BrC has insignificant absorption ($AAE_{BC} = 1$) at longer wavelengths (e.g., 950 and 880 nm), the residual absorption by BrC (b_{abs_BrC}) was calculated by deducting the absorption by BC (b_{abs_BC}) from the overall b_{abs} at the shorter wavelengths (660, 590, 520, 470, 370 nm) (Liu *et al.* 2015; Chen *et al.* 2020).

$$b_{abs_BC}(\lambda) = b_{abs(880)} \times \left(\frac{\lambda}{880}\right)^{-AAE_{BC}}, \quad (10)$$

$$b_{abs_BrC}(\lambda) = b_{abs}(\lambda) - b_{abs_BC}(\lambda). \quad (11)$$

The R-statistical code (R core Team 2021) was used for data analysis and visualization with packages such as ‘openair’, ‘ggplot2’, ‘ggpubr’. All the packages can be retrieved through the Comprehensive R Archive Network (source link: <https://cran.r-project.org/>). The probable source provinces adding to the total BC_{880} concentration at the monitoring site were recognized using the Bivariate polar plots. Multivariate linear correlation analysis was used to reveal the statistically significant parameters.

3. Results

Descriptive information of total BC_{880} , BC_{BB_880} , BC_{FF_880} , b_{abs_BrC} , spectral dependence from the AE-33 measurements, and local meteorological conditions during various lockdowns are listed in table 1. The time-based and daily variations in the BC_{880} mass concentrations are presented in figure 2(a, b), respectively. The BC_{880} concentration ranged from 1.57 to 15.60 $\mu\text{g m}^{-3}$, with a mean concentration of $5.75 \pm 4.24 \mu\text{g m}^{-3}$. The maximum concentration was in the Pre-LD and the minimum in LD4. The average BC_{880} concentrations during Pre-LD, LD1, LD2, LD3, LD4, and Post-LD were 9.29, 4.70, 3.41, 3.69, 2.94, and 6.56 $\mu\text{g m}^{-3}$, individually. The BC_{880} concentration during the Pre-LD period was comparable to the values reported in Delhi (Goel *et al.* 2021). However, during LD1, LD2, LD3, LD4, and Post-LD, the BC_{880} concentration reduced by $\sim 49\%$, $\sim 63\%$, $\sim 60\%$, $\sim 68\%$, and $\sim 29\%$, respectively. The anthropogenic activities such as public transportation and essential industries were relaxed in succeeding lockdowns (stage-wise). The stage-wise easing implemented in different lockdowns dominated the BC_{880} concentration from fossil fuel-associated emissions. Though, after LD3, the BC_{880} concentrations declined due to rain events and the abundant WS. The rainy and windy May and June decreased the BC_{880} and PM concentrations (table 1). BC_{880} concentration’s evening and morning peaks also significantly dropped (62% and 75%) to low (nearly 2 $\mu\text{g m}^{-3}$) during the LD period. After LD4, the evening and morning peaks again started recurring due to relaxation given in anthropogenic activities. However, in the Pre-LD and Post-LD periods, the strength of both evening and morning peaks was high, up to $\sim 14 \mu\text{g m}^{-3}$, because of heavy vehicular activities and emissions.

$AAE_{370-880}$ values were 1.01–1.66 (mean: 1.25 ± 0.08) (figure 3b), which is lesser than the AAE over Delhi during lockdown (1.32 ± 0.16) (Goel *et al.* 2021) and during wintertime (1.29 ± 0.08) (Dumka *et al.* 2018), and was more than (Tiwari *et al.* 2015) for December 2011–March 2012 (1.09 ± 0.11). The average $AAE_{370-880}$ during Pre-LD, LD1, LD2, LD3, LD4, and Post-LD were 1.19, 1.38, 1.33, 1.26, 1.21, and 1.20, respectively. The higher $AAE_{370-880}$ throughout LD1, LD2, and LD3 show the notable contributions from domestic cooking and fire events, and small $AAE_{370-880}$ during Pre-LD, LD4, and Post-LD indicate the most contribution from fossil fuel

Table 1. Summary of the parameters. The values indicate the daily-averaged mean value \pm standard deviation. The surface-reaching solar radiation shows the seven sunshine hours averaged value.

Parameters	Pre-LD	LD1	LD2	LD3	LD4	Post-LD	Overall
BC_{880} ($\mu\text{g m}^{-3}$)	9.29 \pm 4.11	4.70 \pm 0.95	3.41 \pm 0.56	3.69 \pm 1.50	2.94 \pm 0.93	6.56 \pm 5.35	5.75 \pm 4.24
$BC_{FF,880}$ ($\mu\text{g m}^{-3}$)	7.28 \pm 3.41	2.39 \pm 0.54	1.94 \pm 0.21	2.37 \pm 0.79	2.14 \pm 0.54	5.03 \pm 4.59	4.13 \pm 2.65
$BC_{BB,880}$ ($\mu\text{g m}^{-3}$)	2.00 \pm 0.97	2.32 \pm 0.78	1.47 \pm 0.46	1.33 \pm 0.77	0.80 \pm 0.44	1.53 \pm 1.01	1.63 \pm 0.82
FF ₈₈₀ fraction in BC_{880} (%)	78 \pm 10	51 \pm 18	58 \pm 15	66 \pm 18	74 \pm 11	76 \pm 15	70 \pm 12
BB ₈₈₀ fraction in BC_{880} (%)	22 \pm 6	49 \pm 11	42 \pm 9	34 \pm 11	26 \pm 7	24 \pm 9	30 \pm 12
$b_{\text{abs},370}$ (Mm^{-1})	210.28 \pm 88.25	122.63 \pm 28.39	85.60 \pm 17.12	88.72 \pm 39.23	66.56 \pm 23.78	184.88 \pm 111.73	141.52 \pm 88.74
$b_{\text{abs},880}$ (Mm^{-1})	75.40 \pm 31.98	36.54 \pm 7.41	26.46 \pm 4.34	28.70 \pm 11.65	22.81 \pm 7.26	65.64 \pm 41.60	48.51 \pm 32.96
$b_{\text{abs},370,BC}$ (Mm^{-1})	179.33 \pm 76.07	86.92 \pm 17.64	62.94 \pm 10.32	68.28 \pm 27.71	54.27 \pm 17.27	156.13 \pm 98.94	115.37 \pm 78.41
$b_{\text{abs},370,BC}$ (Mm^{-1})	30.94 \pm 15.05	35.72 \pm 12.06	22.67 \pm 7.09	20.45 \pm 11.90	12.30 \pm 6.80	28.76 \pm 15.67	26.15 \pm 14.04
AAE ₃₇₀₋₈₈₀	1.19 \pm 0.05	1.38 \pm 0.06	1.33 \pm 0.05	1.26 \pm 0.07	1.21 \pm 0.03	1.20 \pm 0.05	1.25 \pm 0.08
AAE ₄₇₀₋₉₅₀	1.23 \pm 0.03	1.38 \pm 0.04	1.33 \pm 0.03	1.28 \pm 0.04	1.26 \pm 0.02	1.23 \pm 0.02	1.28 \pm 0.06
Temperature ($^{\circ}\text{C}$)	20.57 \pm 1.03	21.86 \pm 1.64	23.59 \pm 0.88	22.80 \pm 1.94	25.02 \pm 1.17	26.94 \pm 1.44	23.31 \pm 2.66
Humidity (%)	81.35 \pm 6.17	77.87 \pm 7.03	75.84 \pm 4.00	82.19 \pm 16.20	85.83 \pm 2.28	80.34 \pm 6.20	80.66 \pm 7.92
Wind speed (m s^{-1})	0.99 \pm 0.36	1.91 \pm 1.21	2.38 \pm 0.61	2.11 \pm 0.63	1.79 \pm 0.25	1.62 \pm 0.31	1.69 \pm 0.77
Wind direction ($0-360^{\circ}$)	190.60 \pm 58.58	141.41 \pm 17.34	134.32 \pm 27.41	139.65 \pm 45.07	108.92 \pm 54.85	65.76 \pm 10.01	142.37 \pm 57.07
Pressure (mbar)	757.73 \pm 1.21	755.11 \pm 0.59	755.88 \pm 1.06	754.53 \pm 1.20	754.51 \pm 1.33	752.18 \pm 0.58	755.17 \pm 2.18
Solar radiation (W m^{-2})	120.45 \pm 34.99	160.00 \pm 14.74	149.21 \pm 28.83	144.54 \pm 44.68	173.78 \pm 36.82	176.52 \pm 52.56	151.09 \pm 42.24

burning causes. The AAE₄₇₀₋₉₅₀ ranged from 1.05 to 1.59 (mean: 1.28 ± 0.06) (figure 3a). The average AAE₄₇₀₋₉₅₀ values during Pre-LD, LD1, LD2, LD3, LD4, and Post-LD were 1.23, 1.38, 1.33, 1.28, 1.26, and 1.23.

The segregation of two sources was done via 370–880 nm pair and estimated AAE_{FF} and AAE_{BB} of 1 and 1.7, respectively. Figure 4(a and b) shows the results. The daily mean $BC_{FF,880}$ concentration was wide-ranging from 1.21 to $11.30 \mu\text{g m}^{-3}$, with a mean concentration of $4.13 \pm 2.65 \mu\text{g m}^{-3}$. The average $BC_{FF,880}$ mass concentrations throughout Pre-LD, LD1, LD2, LD3, LD4, Post-LD were 7.28, 2.39, 1.94, 2.37, 2.14, $5.03 \mu\text{g m}^{-3}$, respectively. The $BC_{FF,880}$ mass concentration was maximum during Pre-LD and Post-LD. There were no constraints on industrial, vehicular, or additional anthropogenic activities (figure 4a). The $BC_{FF,880}$ was reduced to 67% in LD1 and 74% in LD2. During the lockdowns, the movement of pooled vehicles was restricted except those for essential services such as doctors, police, and other essential commodities. The daily averaged $BC_{BB,880}$ concentration wide-ranging from 0.37 to $4.30 \mu\text{g m}^{-3}$, with a mean concentration of $1.63 \pm 0.82 \mu\text{g m}^{-3}$. The average $BC_{BB,880}$ concentrations during Pre-LD, LD1, LD2, LD3, LD4, Post-LD were 2.00, 2.32, 1.47, 1.33, 0.80, and 1.53, respectively. The $BC_{BB,880}$ concentration was great during LD1 and LD2 due to the forest fire events in the neighbouring region. During LD4, a sudden decrease in $BC_{BB,880}$ concentrations could be attributed to rain events and an increased proportion of vehicular emission, change in WD, and high WS (table 1). Diurnal variation in $BC_{FF,880}$ and $BC_{BB,880}$ concentrations are shown in figure 5(a and b). High $BC_{FF,880}$ mass concentration ($12-18 \mu\text{g m}^{-3}$) was detected during the morning rush hour (9:00–10:00 LST) during the Pre-LD period. From LD1 to LD4, morning and evening peaks ($3-6 \mu\text{g m}^{-3}$) were also witnessed, which could be due to the hospitals, Narayana Super Specialty and GNRC, located within 1 km radius.

The influence of biomass and fossil fuel burning on the overall BC_{880} during Pre-LD, LD1, LD2, LD3, LD4, and post-LD are shown in figure 4(b). The fraction of FF was high during Pre-LD, LD4, and Post-LD, i.e., 78%, 74%, and 76%, respectively. The large fraction of FF during Pre-LD is due to no limitation on anthropogenic activities such as industrial, vehicular, railway, etc. In Post-LD, the fraction of FF was similar to Pre-LD due to

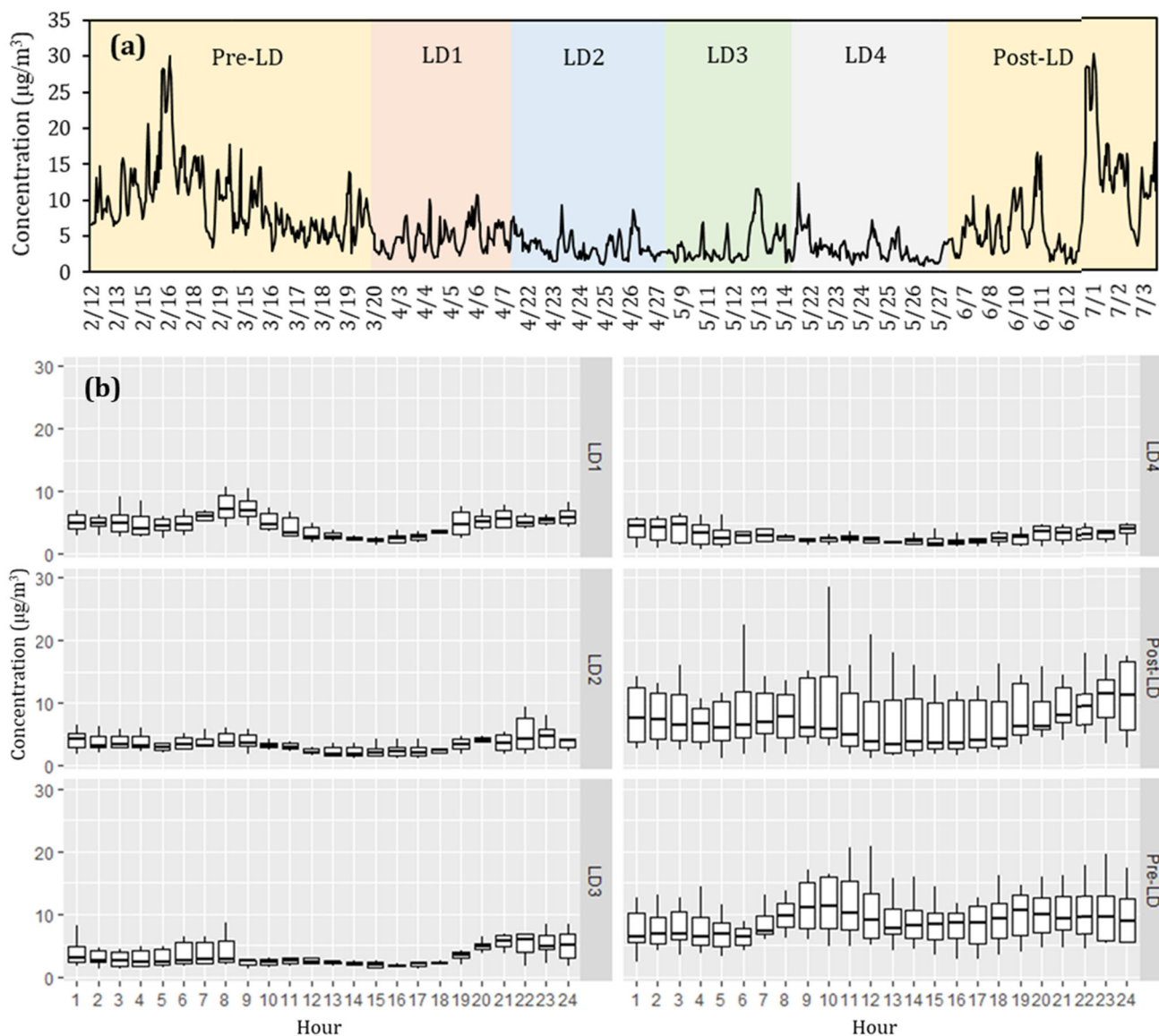


Figure 2. (a) Daily-averaged hourly BC₈₈₀ mass concentration – each colour represents different phases of lockdown. (b) Box plot of the diurnal variation of BC₈₈₀ mass concentration during the study period.

the easing given during this period. In Post-LD, the Indian railway was not functioning, which subsequently directed to the growth of unattended vehicles. Moreover, being the gateway to northeast India, every vehicle passes through Guwahati city to other regions. From LD1 to Post-LD, an increasing FF fraction was observed due to easing in consecutive lockdown and unlock. The fire events might influence BB fraction, which was confirmed by the MODIS satellite retrieved fire data. In northeast India, forest fires are significant biomass burning sources, as revealed in figure S4(a–f). The fire spot data (combined product from Terra and Aqua MCD 14 ML) was collected from the Fire Information for Resources Management System ([https://firms.modaps.](https://firms.modaps.eosdis.nasa.gov/)

[eosdis.nasa.gov/](https://firms.modaps.eosdis.nasa.gov/)). Though, a distinct drift was observed in the fraction of BB, which was highest during LD1 and lowest in Post-LD, the fraction of BB was large during LD1 and LD2 due to decreased vehicular emission in LD1 and increased fire events during LD2. Monthly and phase-wise changes in BC₈₈₀, BC_{FF_880}, and BC_{BB_880} concentration and their changes during various phases are shown in figure 6. The quantitative analysis of phase-wise anomaly was organized to comprehend BC's spatial dissimilarity, sources, and radiation effects compared to the study period mean (figure S2).

Bivariate polar concentration plots of BC₈₈₀, BC_{FF_880}, BC_{BB_880}, and AAE₃₇₀₋₈₈₀, show the conjugate effect of WS, WD, and potential source

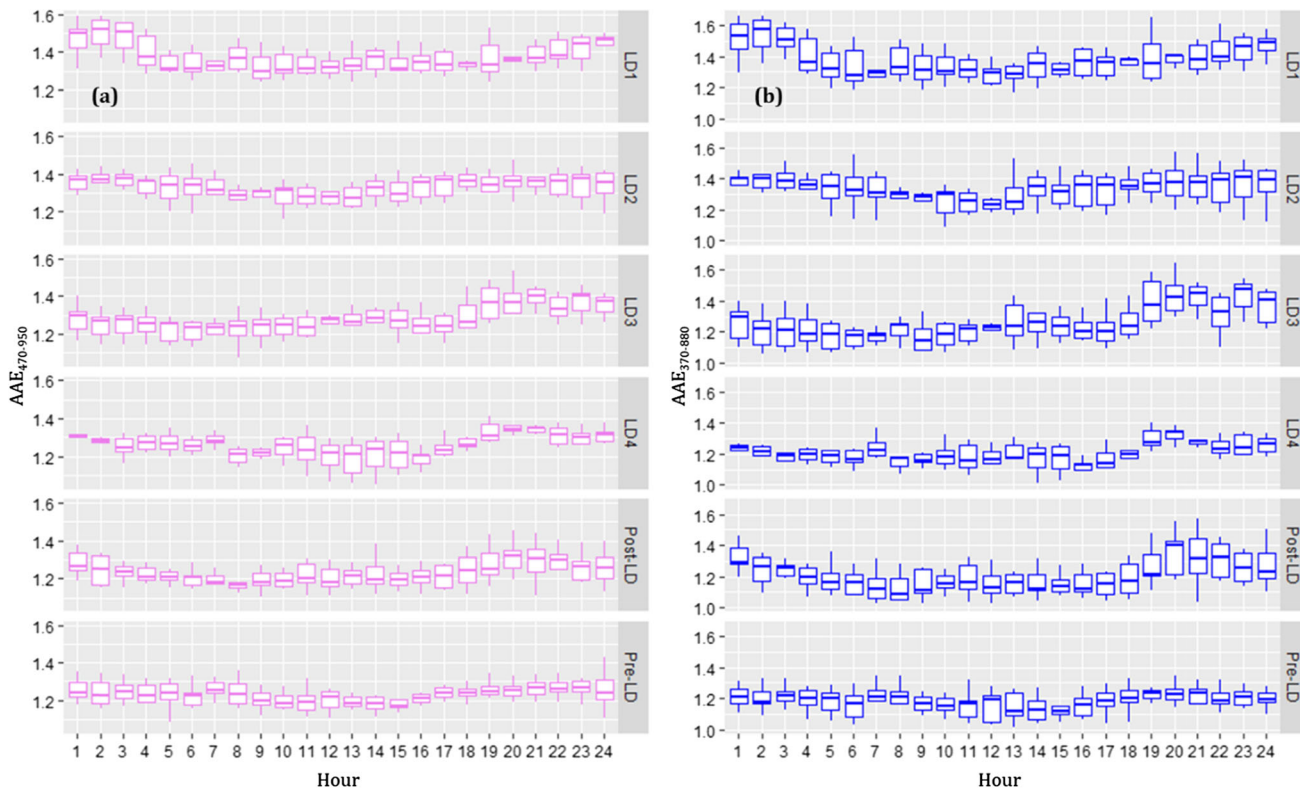


Figure 3. Diurnal variation of AAE₄₇₀₋₉₅₀ (left), and AAE₃₇₀₋₈₈₀ (right).

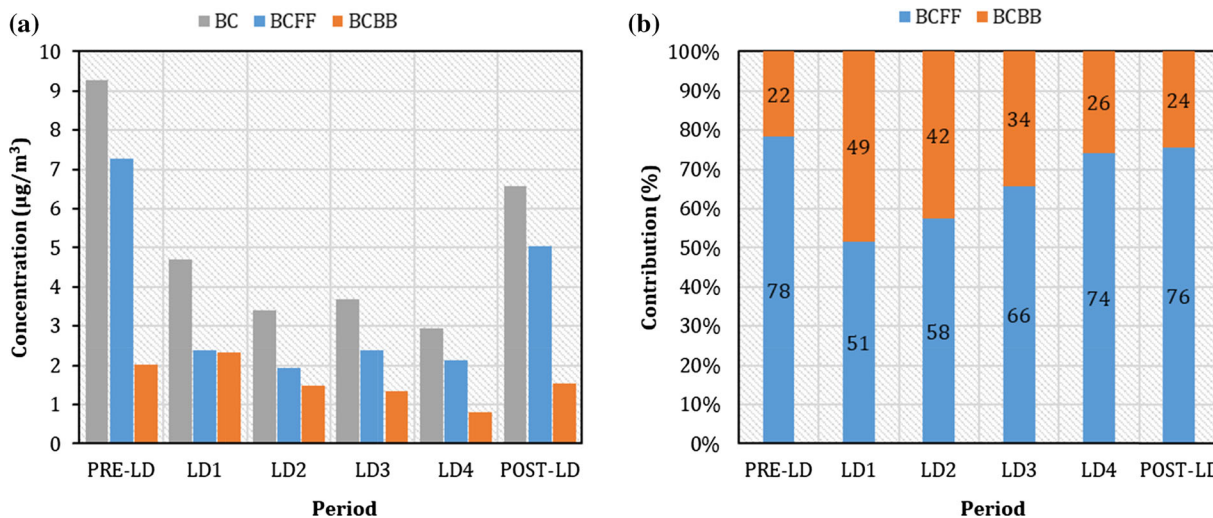


Figure 4. (a) Concentration of BC₈₈₀, BC_{FF,880}, and BC_{BB,880}, and (b) contribution of the two sources to the overall BC₈₈₀ throughout lockdowns.

locations affecting the receptor (figure 7). The mean synoptic shallow wind fields were from the southeast (figure S3). The almost stagnant atmosphere with weak winds ($<2 \text{ m s}^{-1}$) and high pressure (765 bar) enabled subsiding and massive aerosol (BC) build-up near the surface. The maximum AAE₃₇₀₋₈₈₀ values are linked with lower wind speeds from the southwest. The bivariate plots

disclose the domination of the local emission sources as the ultimate BC₈₈₀, BC_{FF,880}, BC_{BB,880} concentrations were related with the low WS from the eastern direction towards the monitoring station. The east region corresponds to the heavily occupied Guwahati suburbs and neighbouring rural agricultural areas, having high traffic and biomass burning. South-easterly wind inflow directions

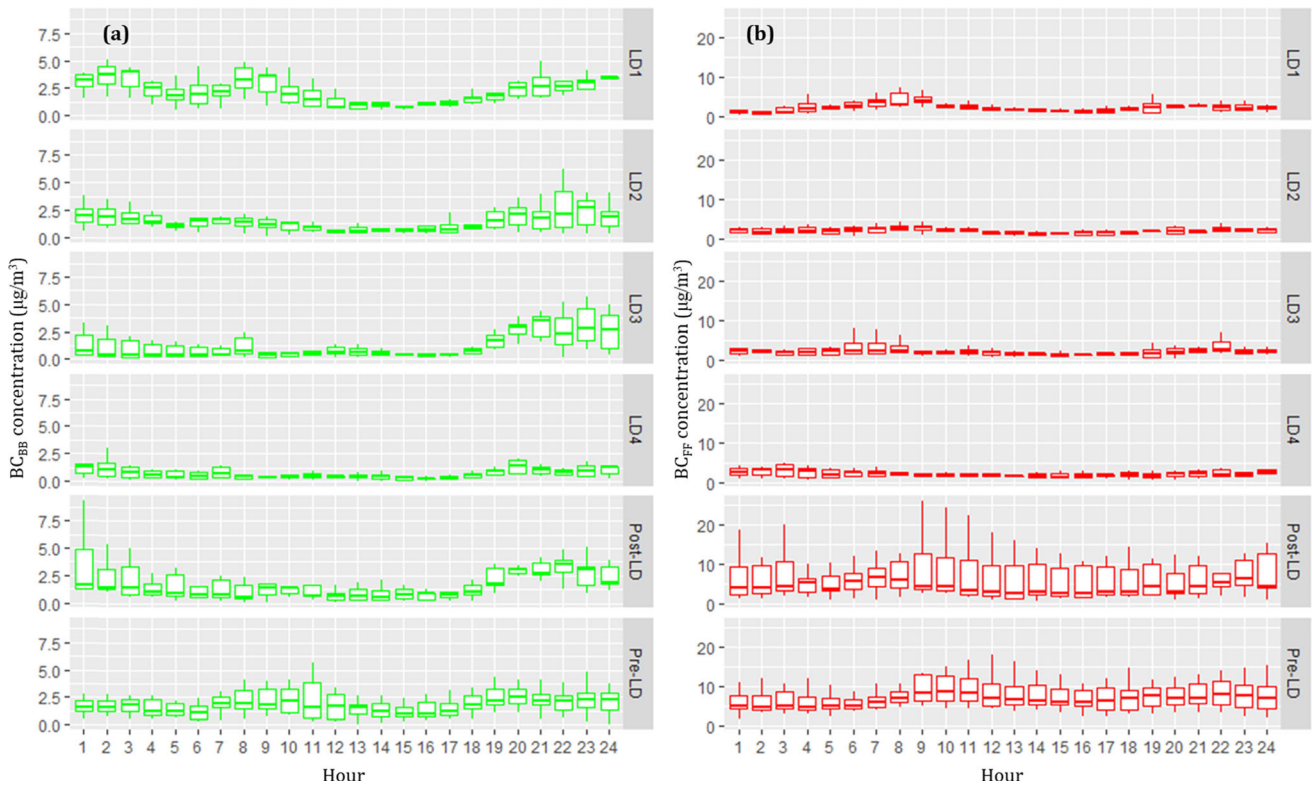


Figure 5. Diurnal variation of $BC_{BB,880}$ (left), and $BC_{FF,880}$ (right).

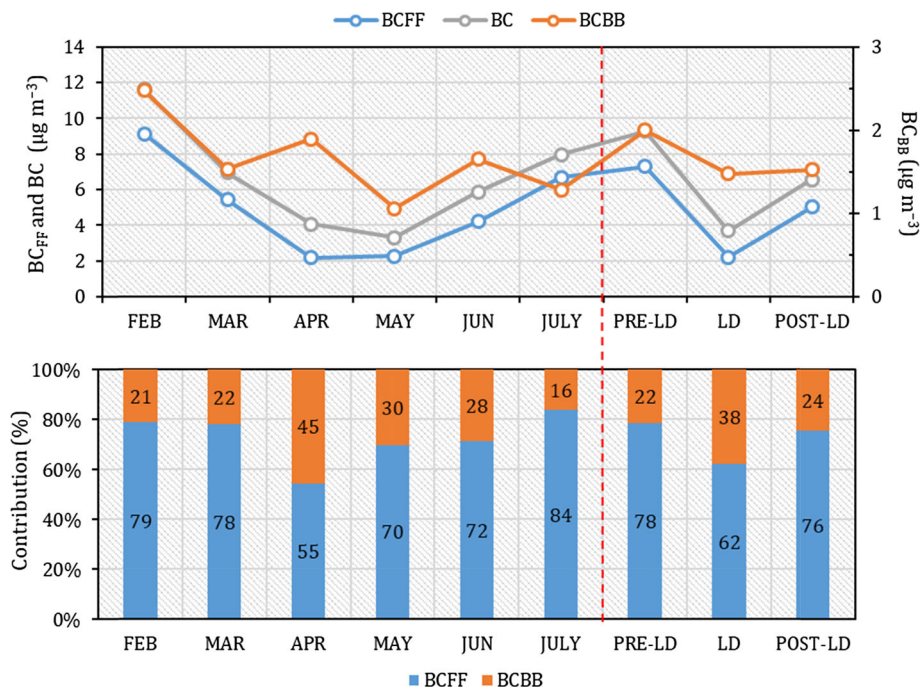


Figure 6. Monthly and phase-wise (lockdown) changes in BC_{880} concentrations and contribution of FF and BB in total BC_{880} .

were dominant over this region, with a mean WS of 1.68 m s^{-1} . During the sampling period, the daily mean temperature varied from 18.88° to 29.17°C (mean: 23.31 ± 2.66). It is described in figure 8 that the BC_{880} mass concentrations were diminished

due to rainy events. Relative humidity correlates substantially with BC_{880} , while T, WS, RF, and SR were negatively associated (figure 9). Rainfall played a significant role in dipping $BC_{BB,880}$ concentration in LD3 to post-LD as more significant

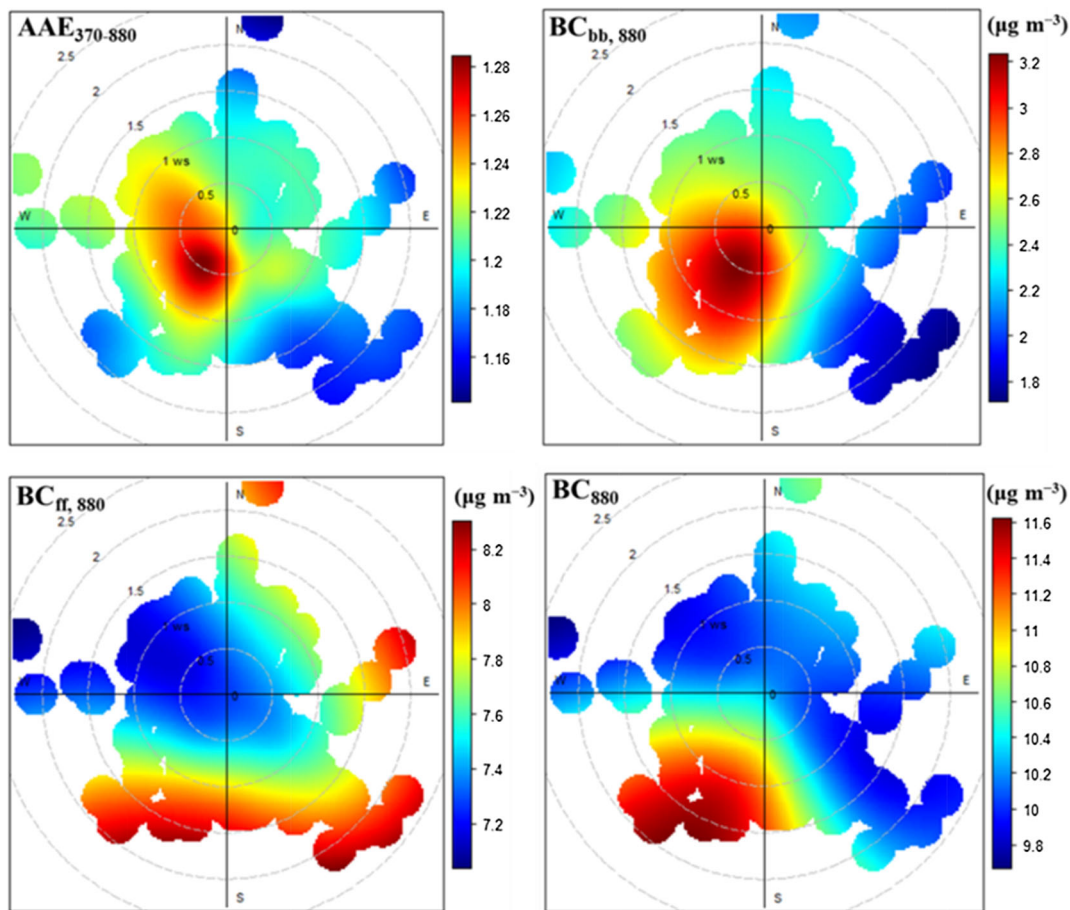


Figure 7. The bivariate polar plot indicates wind fields' effect on the measured $AAE_{370-880}$, $BC_{BB,880}$, $BC_{FF,880}$, and BC_{880} concentrations.

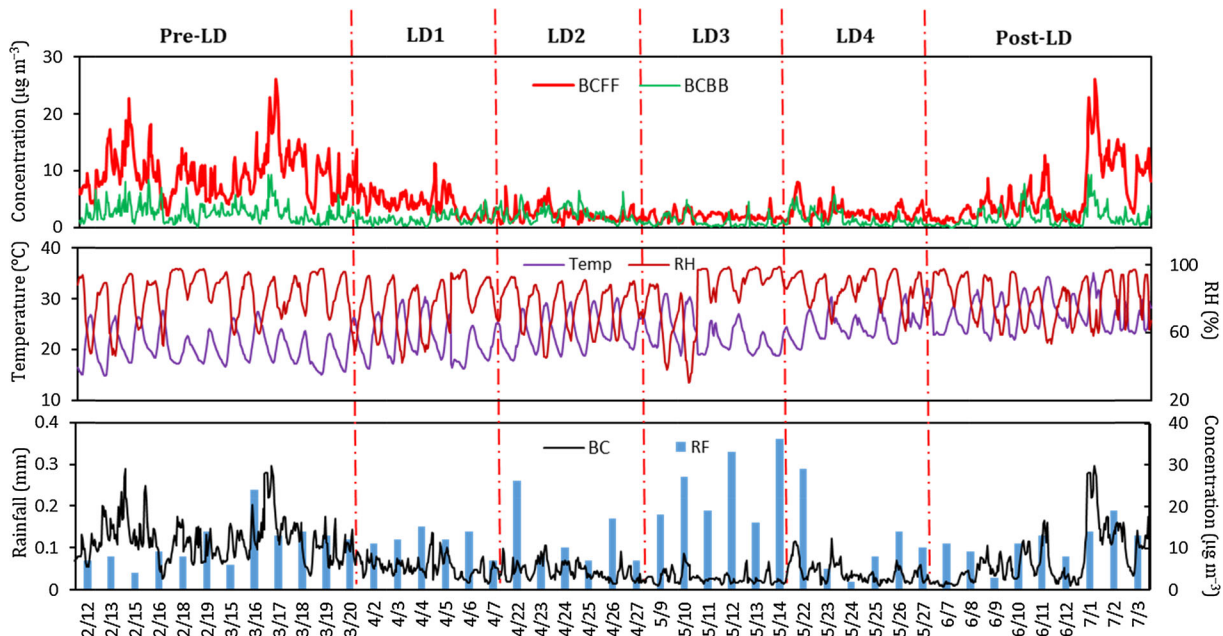


Figure 8. Temporal variations in $BC_{FF,880}$, $BC_{BB,880}$, and BC_{880} mass concentration with the rainfall, temperature, and relative humidity. Rainfall denotes the daily averaged values.

fire events occurred in March and April (figure S4a–f). Figures 8 and 9 indicate the considerable impact of meteorological parameters on BC_{880} concentration in this region before and during the lockdown period.

Variation in radiation effect during lockdowns is shown in figure 10. The average b_{abs} (370 nm) was

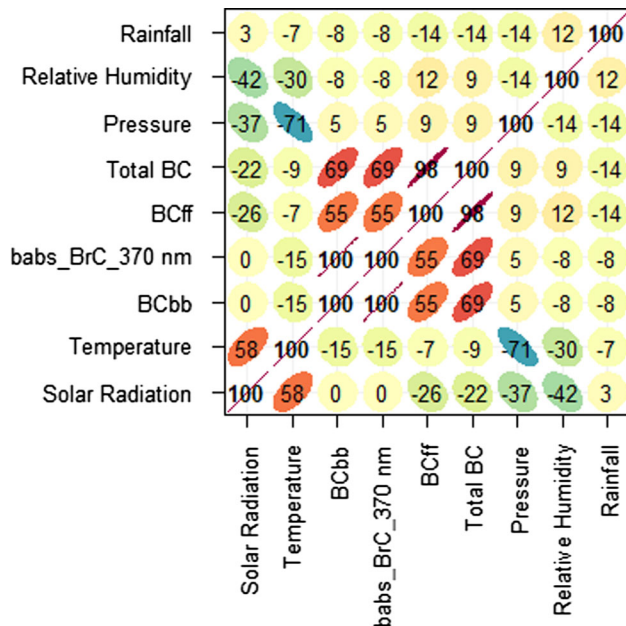


Figure 9. Correlation plot between different parameters. Warm colors show a positive correlation, and cool colors show a negative correlation. For zero correlation, the shape becomes a circle.

$210.28 \pm 88.25 \text{ Mm}^{-1}$, with $122.63 \pm 28.39 \text{ Mm}^{-1}$, $85.60 \pm 17.12 \text{ Mm}^{-1}$, $88.72 \pm 39.23 \text{ Mm}^{-1}$, $66.57 \pm 23.78 \text{ Mm}^{-1}$, $184.88 \pm 111.73 \text{ Mm}^{-1}$ Pre-LD, at LD1, at LD2, at LD3, at LD4, and Post-LD, separately (table 1). The $b_{abs,370}$ was higher than in Chongqing, China ($113 \pm 31.4 \text{ Mm}^{-1}$) during the COVID-19 epidemic (Chen *et al.* 2020). The average b_{abs} (at 880 nm) was $75.40 \pm 31.98 \text{ Mm}^{-1}$, $36.54 \pm 7.41 \text{ Mm}^{-1}$, $26.46 \pm 4.34 \text{ Mm}^{-1}$, $28.70 \pm 11.65 \text{ Mm}^{-1}$, $22.81 \pm 7.26 \text{ Mm}^{-1}$, and $65.64 \pm 41.60 \text{ Mm}^{-1}$ during Pre-LD, at LD1, LD2, LD3, LD4 and Post-LD, respectively (table 1). Also, lockdown actions reduced $b_{abs,880}$ and $b_{abs,370}$ considerably to 72% and 69%, respectively, till LD4. Equally, BC and BrC were the effective sunlight absorber at several wavelengths, while BC was dominant from 370 to 880 nm. The average $b_{abs,BrC}$ (370 nm) was 30.94 ± 15.05 , 35.72 ± 12.06 , 22.67 ± 7.09 , 20.45 ± 11.90 , 12.30 ± 6.80 , 28.76 ± 15.67 , $26.15 \pm 14.04 \text{ Mm}^{-1}$, respectively, during different phases (table 1). The attribution to BrC and BC at various wavelengths between 370 and 880 nm is observed in figure 10. BrC accounted for $\sim 15\%$ of the overall b_{abs} at short wavelength (370 nm) earlier LD1, increased up to $\sim 30\%$ during consecutive lockdowns, and then decreased to 16% during Post-LD. The portion of $b_{abs,BrC,370}$ was considerably lower than in Chongqing (during lockdown) and Guangzhou (in winter), China (Qin *et al.* 2018; Chen *et al.* 2020).

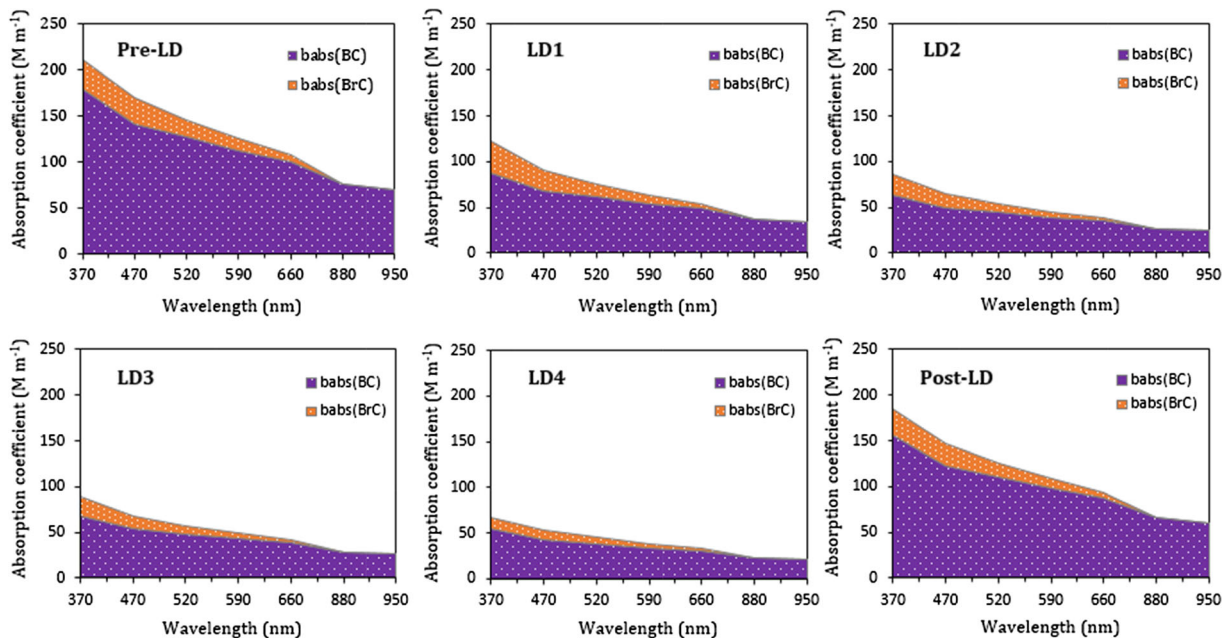


Figure 10. Radiation effect of BC and BrC for the 370–950 nm in the different lockdowns.

4. Discussion

The effect of lockdowns and their related levels of BC_{880} has been assessed in this study to conclude the link between the concentration of BC_{880} and emission sources. Therefore, various phases of lockdowns with pre-lockdown and post-lockdown have been selected purposively. After the announcement of lockdown 1, anthropogenic and industrial activities were completely shut down all over India. Though there was a massive decline in energy use, $PM_{2.5}$, PM_{10} , CO, NO_2 during the initial lockdown (March 16 to April 14, 2020) were decreased around 43, 31, 10, and 18%, respectively, in India from 2017 to 2020 (Sharma *et al.* 2020). Another study conducted in Delhi during March 3–April 14, 2020 by considering 34 monitoring stations showed an essential reduction in PM_{10} (60%), $PM_{2.5}$ (39%), CO (30.35%) and NO_2 (52.68%), and national air quality index improved by 40–50% (Mahato *et al.* 2020). There was a 17% increase in ozone in Delhi (Sharma *et al.* 2020); a possible reason might be due to lower NO_x and volatile organic compounds (VOCs) in urban locations due to a sudden decrease in vehicular activities. The life-threatening lockdowns had affected the economy globally but helped improve air quality during the period, which started to deteriorate again when the lockdown was successively lifted (Chauhan and Singh 2020; Chowdhuri *et al.* 2020; Kumari and Toshniwal 2020; Mahato *et al.* 2020; Sharma *et al.* 2020; Goel *et al.* 2021). A study conducted by Barman and Gokhale (2019) in the City Center (Guwahati) and in the residential area having much less commercial and vehicular activities than at the City Center has found the BC concentration values of 17.14 and 6.42 $\mu g m^{-3}$ during pre-monsoon (2017), respectively, which were too high as compared with the value found in this study (i.e., 3.68 $\mu g m^{-3}$). Further, in winter (January, February), the values are even higher due to unfavourable meteorology. Therefore, the significant decrease in the values recorded in this study during the lockdown period has been the result of no anthropogenic activities and not the effect of seasonal transformation. This study showed that BC_{880} concentration was dropped up to 68%, and BrC accounted for 25% of the b_{abs} at 370 nm during the lockdowns.

In the study region, the hilly topography may have also promoted the accumulation of black carbon due to poor dispersion. At the same time, the reduction was not as effective as the other

studies reported in India and other parts of the world (Chen *et al.* 2020; Sharma *et al.* 2020; Saxena and Raj 2021; Zhang *et al.* 2021). Moreover, other parts of the country experienced a significant reduction in the AOD during distinct stages of lockdown. At the same time, the changes in AOD in northeastern India were minimal (Ranjan *et al.* 2020). This study revealed that the IGPs (e.g., Uttarakhand) had a more significant affirmative influence of lockdown, where the AOD level diminished to $\sim 43\%$ throughout the lockdowns.

BC's deposition and transport significantly affected this region due to rain events and calm wind conditions. The BC_{880} concentrations might also have been affected by the terrain of this region and may also further have influenced the probability of fog occurrence (Hunová *et al.* 2021). Moreover, a study by Goel *et al.* (2021) in Delhi reported a reduction of 78% in BC_{880} mass concentration during the lockdowns, and it was 68% in the present study. Hence, region-specific and restricted emission control policies should be applied to air quality management for sustainable development. This study focuses on black carbon aerosols, their sources, and the light absorption properties of BC and BrC. It also provides the assessment to determine the effect of an epidemic with its control during the lockdown periods in the region. While many studies carried out in India and other areas during the pandemic period were mainly focused on the reduction of air pollutants ($PM_{2.5}$, PM_{10} , SO_2 , NO_2 , O_3 , and BC) during a few lockdowns (Chauhan and Singh 2020; Chen *et al.* 2020; Mahato *et al.* 2020; Goel *et al.* 2021; Sharma *et al.* 2020; Saxena and Raj 2021), this study provides the knowledge on the impact on BC_{880} emission sources and the ambient BC_{880} concentrations. The sudden decrease in the BC_{880} concentrations during the various lockdown phases showed that the control at the origins of anthropogenic activities could improve air quality. And therefore, the imposing lockdown helped lessen coronavirus spread and improved the region's air quality significantly.

5. Conclusion

The longtime lockdown during the COVID-19 pandemic showed that direct control at the sources could reduce air pollution significantly. The BC_{880} mass concentration decreased by 49%, 63%, 60%, 68%, and 29% successively in the various phases of

lockdowns. An improved method of source apportionment showed a significant variation in the contribution of BC_{880} sources; for example, the share of fossil fuel sources in the total BC_{880} was the lowest in LD1, which continues to increase due to successive easing in the shutdown of activities. The BC_{FF_880} fraction was found to be reduced from 0.78 to 0.51. During March and April, the natural forest fire events increased the fraction of biomass burning in BC_{880} during the first two lockdowns. At several bands, the aerosol absorption coefficient declined by 69%, and AAE was reduced by 64% during lockdowns. BrC played a significant share in light absorption, accounting for 25% of b_{abs} at 370 nm. Thus, this study revealed a substantial reduction in BC_{BB_880} , BC_{FF_880} , total BC_{880} over BRV, and significant changes in aerosol absorption coefficients due to the proportion of black and brown carbons. The results may be helpful as baseline data to study the impacts of sources on the contribution to atmospheric BC and mitigations strategies.

Acknowledgements

This study is supported by Science and Engineering Research Board, Department of Science and Technology (DST), Government of India (Grant No: EMR/2014/001039), and the financial support from the Department of Civil Engineering, Indian Institute of Technology Guwahati, Assam. The authors also gratefully acknowledge the Air & Noise Pollution Laboratory of IIT Guwahati for providing the necessary data and support.

Author statement

Sameer Singh: Fieldwork, data analysis, and writing the original draft. Sharad Gokhale: Supervision, resources, validation, writing, and manuscript review.

References

- Ahmed W, Angel N, Edson J, Bibby K, Bivins A, O'Brien J W, Choi P M, Kitajima M, Simpson S L, Li J and Tscharke B 2020 First confirmed detection of SARS-CoV-2 in untreated wastewater in Australia: A proof of concept for the wastewater surveillance of COVID-19 in the community; *Sci. Total Environ.* **728** 138764.
- Banerjee A, Kulcsar K, Misra V, Frieman M and Mossman K 2019 Bats and coronaviruses; *Viruses* **11** 41.
- Barman N and Gokhale S 2019 Urban black carbon-source apportionment, emissions, and long-range transport over the Brahmaputra River Valley; *Sci. Total Environ.* **693** 133577.
- Beyer R M, Manica A and Mora C 2021 Shifts in global bat diversity suggest a possible role of climate change in the emergence of SARS-CoV-1 and SARS-CoV-2; *Sci. Total Environ.* **767** 145413.
- Bond T C and Bergstrom R W 2006 Light absorption by carbonaceous particles: An investigative review; *Aerosol Sci. Technol.* **40** 27–67.
- Chakrabarty R K, Garro M A, Wilcox E M and Moosmüller H 2012 Strong radiative heating due to wintertime black carbon aerosols in the Brahmaputra River Valley; *Geophys. Res. Lett.* **39**(9).
- Chauhan A and Singh R P 2020 Decline in $PM_{2.5}$ concentrations over major cities around the world associated with COVID-19; *Environ. Res.* **187** 109634.
- Chen Y, Zhang S, Peng C, Shi G, Tian M, Huang R J, Guo D, Wang H, Yao X and Yang F 2020 Impact of the COVID-19 pandemic and control measures on air quality and aerosol light absorption in Southwestern China; *Sci. Total Environ.* **749** 141419.
- Chowdhuri I, Pal S C, Saha A, Chakraborty R, Ghosh M and Roy P 2020 Significant decrease of lightning activities during COVID-19 lockdown period over Kolkata megacity in India; *Sci. Total Environ.* **747** 141321.
- Drinovec L, Mocnik G, Zotter P, Prévôt A S H, Ruckstuhl C, Coz E, Rupakheti M, Sciare J, Müller T, Wiedensohler A and Hansen A D A 2015 The 'dual-spot' Aethalometer: An improved measurement of aerosol black carbon with real time loading compensation; *Atmos. Tech.* **8** 1965–1979.
- Dumka U C, Kaskaoutis D G, Tiwari S, Safai P D, Attri S D, Soni V K, Singh N and Mihalopoulos N 2018 Assessment of biomass burning and fossil fuel contribution to black carbon concentrations in Delhi during winter; *Atmos. Environ.* **194** 93–109.
- Economic survey of Assam 2017–18 Transportation and development department Government of Assam 2018 (<https://des.assam.gov.in/information-services/economic-survey-assam>).
- Evans M, Kholod N, Kuklinski T, Denysenko A, Smith S J, Staniszewski A, Hao W M, Liu L and Bond T C 2017 Black carbon emissions in Russia: A critical review; *Atmos. Environ.* **163** 9–21.
- Goel V, Hazarika N, Kumar M, Singh V, Thamban N M and Tripathi S N 2021 Variations in black carbon concentration and sources during COVID-19 lockdown in Delhi; *Chemosphere* **270** 129435.
- Gogoi M M, Krishna Moorthy K, Babu S S and Bhuyan P K 2009 Climatology of columnar aerosol properties and the influence of synoptic conditions: First-time results from the northeastern region of India; *J. Geophys. Res. Atmos.* **114** (D8).
- Gogoi M M, Babu S S, Arun B S, Moorthy K K, Ajay A, Ajay P, Suryavanshi A, Borgohain A, Guha A, Shaikh A and Pathak B 2021 Response of ambient BC concentration across the Indian region to the nation-wide lockdown: Results from the ARFINET measurements of ISRO-GBP; *Curr. Sci.* **120**(2) 341–351.
- Goldreich Y, Druyan L M and Berger H 1986 The interaction of valley/mountain winds with a diurnally veering sea/land breeze; *J. Climatol.* **6**(5) 551–561.

- Han Y, Cao J, Chow J C, Watson J G, An Z, Jin Z, Fung K and Liu S 2007 Evaluation of the thermal/optical reflectance method for discrimination between char-EC and soot-EC; *Chemosphere* **69** 569–574.
- Hunová I, Brabec M, Malý M, Dumitrescu A and Geletič J 2021 Terrain and its effects on fog occurrence; *Sci. Total Environ.* **768** 144359.
- Jansen K L, Larson T V, Koenig J Q, Mar T F, Fields C, Stewart J and Lippmann M 2005 Associations between health effects and particulate matter and black carbon in subjects with respiratory disease; *Environ. Health Perspect.* **113(12)** 1741–1746.
- Jenkins G 2014 A comparison between two types of widely used weather stations; *Weather* **69(4)** 105–110.
- Kumari P and Toshniwal D 2020 Impact of lockdown measures during COVID-19 on air quality – A case study of India; *Int. J. Environ. Health Res.* **32(3)** 503–510.
- Liu D, Taylor J W, Young D E, Flynn M J, Coe H and Allan J D 2015 The effect of complex black carbon microphysics on the determination of the optical properties of brown carbon; *Geophys. Res. Lett.* **42(2)** 613–619.
- Mahato S, Pal S and Ghosh K G 2020 Effect of lockdown amid COVID-19 pandemic on air quality of the megacity Delhi, India; *Sci. Total Environ.* **730** 139086.
- Pathak B, Bhuyan P K, Saikia A, Bhuyan K, Ajay P, Nath S J and Bora S L 2021 Impact of lockdown due to COVID-19 outbreak on O₃ and its precursor gases, PM and BC over northeast India; *Curr. Sci.* **120(2)** 322.
- Qin Y M, Tan H B, Li Y J, Li Z J, Schurman M I and Liu L 2018 Chemical characteristics of brown carbon in atmospheric particles at a suburban site near Guangzhou, China; *Atmos. Chem. Phys.* **18** 16,409–16,418.
- R Core Team 2021 R: A language and environment for statistical computing. R Foundation for Statistical Computing, Vienna, Austria; <https://www.R-project.org/>.
- Ramanathan V and Carmichael G 2008 Global and regional climate changes due to black carbon; *Nat. Geosci.* **1(4)** 221–227.
- Ranjan A K, Patra A K and Gorai A K 2020 Effect of lockdown due to SARS COVID-19 on aerosol optical depth (AOD) over urban and mining regions in India; *Sci. Total Environ.* **745** 141024.
- Sandradewi J, Prévôt A S H, Weingartner E, Schmidhauser R, Gysel M and Baltensperger U 2008 A study of wood-burning and traffic aerosols in an Alpine valley using a multi-wavelength Aethalometer; *Atmos. Environ.* **42(1)** 101–112.
- Saxena A and Raj S 2021 Impact of lockdown during COVID-19 pandemic on the air quality of North Indian cities; *Urban Clim.* **35** 100754.
- Schneider J U, Kirchner S, Borrmann R V and Scheer V 2008 In Situ Measurements of Particle Number Concentration, Chemically Resolved Size Distributions and Black Carbon Content of Traffic-Related Emissions on German Motorways, Rural Roads and in City Traffic; *Atmos. Environ.* **42(18)** 4257–4268.
- Sharma S, Zhang M, Gao J, Zhang H and Kota S H 2020 Effect of restricted emissions during COVID-19 on air quality in India; *Sci. Total Environ.* **728** 138878.
- Singh A and Dey S 2012 Influence of aerosol composition on visibility in megacity Delhi; *Atmos. Environ.* **62** 367–373.
- Singh S and Gokhale S 2021 Source apportionment and light absorption properties of black and brown carbon aerosols in the Brahmaputra River valley region; *Urban Clim.* **39** 100963.
- Stanam A, Chaudhari M and Rayudu D 2020 Effects of temperature on COVID-19 transmission; *Medrxiv.*, <https://doi.org/10.1101/2020.03.29.20044461>.
- Tiwari S, Pipal A S, Srivastava A K, Bisht D S and Pandithurai G 2015 Determination of wood-burning and fossil fuel contribution of black carbon at Delhi, India using aerosol light absorption technique; *Environ. Sci. Pollut. Res.* **22** 2846–2855.
- USEPA 2012 Report to Congress on Black Carbon; *Department of the Interior, and Related Agencies, Issue (March)* 388.
- Van der Zee S C, Fischer P H and Hoek G 2016 Air pollution in perspective: Health risks of air pollution expressed in equivalent numbers of passively smoked cigarettes; *Environ. Res.* **148** 475–483.
- Wang X, Heald C L, Ridley D A, Schwarz J P, Spackman J R, Perring A E, Coe H, Liu D and Clarke A D 2014 Exploiting simultaneous observational constraints on mass and absorption to estimate the global direct radiative forcing of black carbon and brown carbon; *Atmos. Chem. Phys.* **14(20)** 10,989–11,010.
- Westhaus S, Weber F A, Schiwiy S, Linnemann V, Brinkmann M, Widera M, Greve C, Janke A, Hollert H, Wintgens T and Ciesek S 2021 Detection of SARS-CoV-2 in raw and treated wastewater in Germany – suitability for COVID-19 surveillance and potential transmission risks; *Sci. Total Environ.* **751** 141750.
- WHO J N, Gerlofs-Nijland M E, Lanki T, Salonen R O and Cassee F 2012 Health effects of black carbon. Bonn: WHO Regional Office for Europe; *The WHO European Centre for Environ. and Health*.
- Xiao K, Zhai J, Feng Y, Zhou N, Zhang X, Zou J J, Li N, Guo Y, Li X, Shen X and Zhang Z 2020 Isolation of SARS-CoV-2-related coronavirus from Malayan pangolins; *Nature* **583(7815)** 286–289.
- Zhang M, Katiyar A, Zhu S, Shen J, Xia M, Ma J, Kota S H, Wang P and Zhang H 2021 Impact of reduced anthropogenic emissions during COVID-19 on air quality in India; *Atmos. Chem. Phys.* **21(5)** 4025–4037.